Rydberg electromagnetically induced transparency in ^{40}K ultracold Fermi gases

Guoqi Bian (边国旗)[1,2], Biao Shan (单 标)[1,2], Lianghui Huang (黄良辉)[1,2*], and Jing Zhang (张 靖)[1**]

[1] State Key Laboratory of Quantum Optics and Quantum Optics Devices, Institute of Opto-electronics, Shanxi University, Taiyuan 030006, China

[2] Collaborative Innovation Center of Extreme Optics, Shanxi University, Taiyuan 030006, China

*Corresponding author: huanglh06@sxu.edu.cn

**Corresponding author: jzhang74@sxu.edu.cn

We report the measurement of the electromagnetically induced transparency (EIT) with Rydberg states in ultracold ^{40}K Fermi gases, which is obtained through a two-photon process with the ladder scheme. Rydberg–EIT lines are obtained by measuring the atomic losses instead of the transmitted probe beam. Based on the laser frequency stabilization locking to the superstable cavity, we study the Rydberg–EIT line shapes for the 37s and 35d states. We experimentally demonstrate the significant change in the Rydberg–EIT spectrum by changing the principal quantum number of the Rydberg state ($n = 37/52$ and $l = 0$). Moreover, the transparency peak position shift is observed, which may be induced by the interaction of the Rydberg atoms. This work provides a platform to explore many interesting behaviors involving Rydberg states in ultracold Fermi gases.

Keywords: atomic and molecular physics; hyperfine structure; Rydberg states.
DOI: 10.3788/COL202321.100201

1. Introduction

Rydberg atoms display rich many-body behaviors due to their long lifetimes, blockade effect with strong long-range interaction, very large polarizabilities, etc.[1,2]. These novel characteristics led to numerous applications in Rydberg molecules[3–7], nonlinear quantum optics[8,9], quantum simulation[10–16], and quantum information processing[17,18], with controllable interactions using static electric or magnetic, laser or microwave fields.

Rydberg-dressed Bose and Fermi atomic gases display very different many-body phenomena[19,20]. Many phenomena relating to the Rydberg states in an atomic Bose–Einstein condensate have been studied experimentally[21–27]. There are many theoretical works studying Rydberg-dressed Fermi gas[28–31]. Rydberg-dressed interactions between fermionic atoms may resolve puzzles related to strongly correlated electronic solids, such as topological superfluids[32] and topological density waves[33]. The Rydberg states in ultracold Fermi gases are still waiting to be studied and explored in experiment, though the initial work has been carried out recently[34,35].

Electromagnetically induced transparency (EIT) is a useful technique to probe the properties of interacting Rydberg atoms[36] and provides a nondestructive probe of the Rydberg state without actually transferring the population into the Rydberg state[37]. Generally, the EIT spectrum can be obtained in two different ways. The first method is the normal EIT spectrum by measuring the transmission of a probe beam through an atomic sample by scanning its frequency while the frequency of coupling beam is fixed[38,39]. This method results in the standard three-level EIT line shape, which has a narrow transmission window at resonance frequency and strong absorption at two dressed states on both sides of the transmission window. The second method is the unusual EIT spectrum, which is carried out by measuring the probe beam intensity by scanning the frequency of the coupling beam across the atomic transition and keeping the probe laser locked to resonance[40], which can eliminate the Doppler background in thermal vapors[41]; the probe-absorption signal shows transparency peak whenever the coupling laser comes into resonance. The unusual EIT spectrum presents a dark background[42], which seems to be of great benefit for applications such as the measurement with high resolution of hyperfine splitting between excited states[43,44], laser-frequency stabilization[45,46], and the study of highly excited Rydberg states[47–49].

2. Principle and Experimental Setup

In the present work, we apply this technique to detect Rydberg states of ^{40}K ultracold Fermi gases with the ladder scheme shown in Fig. 1(a). We obtain the normal and unusual Rydberg–EIT spectrum in ultracold Fermi gases by measuring the optical density of remaining atoms in the optical trap as a function of the
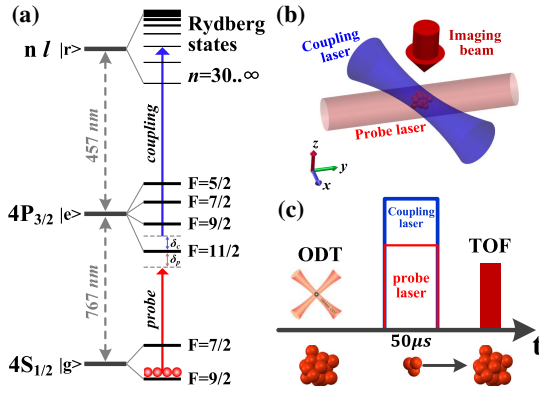
Fig. 1. Experimental setup and procedure. (a) Energy levels of the two-photon Rydberg excitation of ^{40}K. The three energy levels are shown as $|4S_{1/2}, F = 9/2, m_F = 9/2\rangle \equiv |g\rangle \rightarrow |4P_{3/2}, F = 11/2, m_F = 11/2\rangle \equiv |e\rangle \rightarrow |nl\rangle \equiv |r\rangle$, with $l = 0$ (S) or 2 (D). (b) Optical setup. The laser beam for absorption imaging is σ^+-polarized and collimated with a Gaussian waist of 2 cm propagating along the $\hat{z}$. The probe laser polarized linearly along $\hat{x}$ for the EIT propagates along the y axis and is collimated with a Gaussian waist of 2 mm. The coupling laser for exciting from intermediate state $|e\rangle$ to Rydberg states $|r\rangle$ is linearly polarized along $\hat{z}$ with $1/e^2$ radii of 200 μm and illuminates the atom cloud in the x–y plane. (c) Time sequence for the EIT; after applying the probe and coupling light, the atoms ballistically expand to take the TOF absorption image with a CCD.

probe laser detuning and coupling laser detuning, respectively. This work will provide a way to control the interaction through the accurate manipulation of Rydberg states and will explore many unusual behaviors involving Rydberg states in ultracold Fermi gases.

The experimental setup is sketched in Fig. 1(b) and presented in detail in our previous works[50,51]. The experiment starts with the preparation of a degenerate Fermi gas of ^{40}K atoms in the state $|F = 9/2, m_F = 9/2\rangle$ in a crossed optical dipole trap. Around $N = 3 \times 10^6$, ultracold ^{40}K atoms are prepared at a temperature of $0.3T_F$ using sympathetic cooling by ^{87}Rb, where the Fermi temperature is defined by $T_F = \hbar\bar{\omega}(6N)^{1/3}/k_B$. Here $\bar{\omega} = (\omega_x\omega_y\omega_z)^{1/3} \simeq 2\pi \times 80\,\text{Hz}$ is the geometric mean of the optical trap in our experiment, N is the particle number of ^{40}K atoms, and k_B is the Boltzmann's constant. The remaining ^{87}Rb atoms are removed by shining a resonant laser beam pulse (780 nm) for 0.03 ms without heating and losing ^{40}K atoms.

The energy level scheme for the two-photon Rydberg excitation is shown in Fig. 1(a). The three-level ladder system used for EIT includes the ground state $(4S_{1/2})$, the intermediate state $(4P_{3/2})$, and the highly excited Rydberg state $(nS_{1/2}$ or $nD_{3/2,5/2})$, where the energy difference between $nD_{3/2}$ and $nD_{5/2}$ is less than 40 MHz with $n \geq 30$[52]. A weak probe beam with wavelength 767 nm is locked to the transition between $|g\rangle = |F = 9/2, m_F = 9/2\rangle$ state of $4S_{1/2}$ and $|e\rangle = |F' = 11/2, m_{F'} = 11/2\rangle$ state of $4P_{3/2}$. A strong coupling beam drives the transition between the intermediate $|F' = 11/2, m_{F'} = 11/2\rangle$ state of $4P_{3/2}$ and the highly excited Rydberg states $|r\rangle$ of $nS_{1/2}$ or $nD_{3/2,5/2}$ around

457 nm. The coupling laser beam is derived from a system of external cavity diode laser (ECDL)-tapered amplifier (TA) cavity-enhanced second-harmonic generation (SHG) with 800 mW output at 457 nm. The frequency of the coupling laser is measured using a high-resolution wavemeter (HighFinesse, WS7, measurement resolution of 30 MHz). The probe laser polarized linearly along $\hat{x}$ for the EIT is propagated along the y axis and is collimated with a Gaussian waist of 2 mm. The coupling laser for exciting to Rydberg states illuminates the atom cloud in the x–y plane with $1/e^2$ radii of 200 μm, which drives $\sigma^{\pm}$ transitions, depending on whether an ns or nd state is required. The probe and coupling field intensities are around $I_p = 0.16\,\text{mW/cm}^2$ and $I_c = 0.80\,\text{kW/cm}^2$, respectively. The pulse duration and intensity of the probe and coupling laser beams are controlled through acousto-optic modulators (AOMs). The probe and coupling fields are switched on and off simultaneously, and the duration of the pulse is 50 μs, as shown in Fig. 1(c). After exposure to the two fields, the optical dipole trap and the homogeneous magnetic field are switched off simultaneously. This is followed by free flight for 12 ms and taking the time-of-flight (TOF) absorption image with a CCD. As shown in Fig. 1(b), the imaging laser beam for absorption imaging is σ^+-polarized and collimated with a Gaussian waist of 2 cm propagating along the $\hat{z}$.

The frequencies of the probe and coupling lasers are simultaneously locked to a superstable cavity in order to control them accurately and achieve two-photon transition. Here, we employ an additional signal modulation to create a sideband in Pound–Drever–Hall (PDH) locking, as shown in Fig. 2(a). This allows us to tune the laser frequency over a large range[53]. In order to reduce thermal deformation and decrease vibrations, the stabilized ultralow expansion glass cavity (A-T Films) is integrated in a temperature-controlled ultrahigh vacuum and enclosed in a thermal radiation shield. The probe and coupling lasers first pass through a broadband fiber EOM (Ixblue) with a high bandwidth of about 16 GHz, respectively. The modulating signal on the fiber EOM consists of two signals from a microwave signal generator (MW-FG) and a radio-frequency signal generator (RF-FG) combined by a splitter (ZESC-2-11+) to realize the electronic sideband (ESB) locking. Finally, the probe and coupling lasers can be locked to the same superstable cavity using the ESB locking, and tuned with large frequency range via the MW-FG. The ESB error signal and transmitted signal of the phase-modulated 767 nm laser incident on the cavity shown in Fig. 2(b) are obtained by sweeping the carrier frequency of the 767 nm laser. Here, the output signals of MW-FG and RF-FG are 120 and 28 MHz, respectively. In our experiment, both lasers are locked to a stable, high-finesse Fabry–Perot cavity with a free spectral range of 3 GHz. We can estimate the laser linewidths below 80 kHz[54,55].

3. Experiment Analysis

The normal and unusual Rydberg–EIT spectrum profile for a ladder system can be obtained by the complex susceptibility
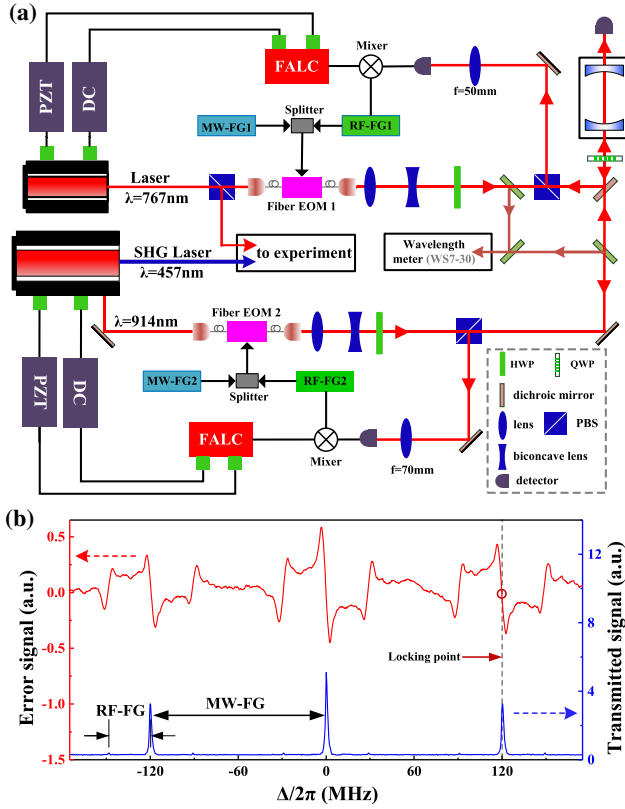
Fig. 2. Schematic of the laser system for 767 and 457 nm. (a) Locking scheme for 767 and 457 nm. The probe laser beam with wavelength 767 nm is produced by an ECDL, which can be locked to the transition between $|F = 9/2, m_F = 9/2\rangle$ state of $4S_{1/2}$ and $|F' = 11/2, m_{F'} = 11/2\rangle$ state of $4P_{3/2}$. The coupling laser beam is derived from a commercial frequency-doubled diode laser system (Toptica TA-SHG pro) providing 800 mW output at 455.5–458.5 nm. In order to improve the frequency stability, the probe and coupling lasers are frequency-locked to a thermally stabilized ultra-low expansion glass cavity via the PDH method. To shift the arbitrary laser frequency detuning of probe and coupling lasers around the resonant transition, we use an additional signal generator to generate a sideband before PDH locking. (b) Transmitted signal of the phase-modulated 767 nm laser (blue curve) on the cavity, which is obtained by sweeping the carrier frequency of the 767 nm laser; the red curve represents the corresponding error signal. Here, the output signals of MW-FG and RF-FG are 120 and 28 MHz, respectively.

in the limit of a weak probe[56], which neglects the Doppler-broadening effect,

$$\chi = \frac{iDd_{eg}^2}{\epsilon_0 \hbar} \left(\gamma_{eg} - i\delta_p + \frac{(\Omega_c/2)^2}{\gamma_{rg} - i(\delta_p + \delta_c)} \right)^{-1}, \quad (1)$$

where D is the optical density of ultracold atomic sample, d_{eg} is the dipole moment matrix element of the transition between $|g\rangle$ and $|e\rangle$, ϵ_0 is the permittivity of vacuum, $\hbar$ is the Planck's constant, δ_p is the probe laser detuning for the transition $|g\rangle \rightarrow |e\rangle$, and δ_c is the coupling laser detuning for the transition $|e\rangle \rightarrow |r\rangle$.
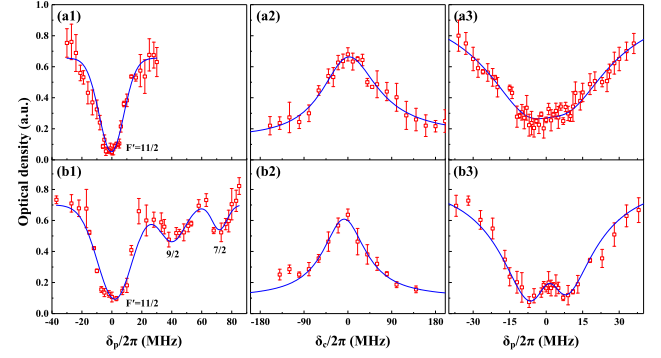

Fig. 3. Measurement of the Rydberg–EIT spectrum. The spectrum as a function of the probe beam detuning δ_p when the weak probe laser is locked to the (a1) SAS and (b1) ultrastable cavity, respectively, in the absence of a coupling laser. The loss profiles correspond to the transition from the $F = 9/2$ state of $4S_{1/2}$ to $|F' = 11/2, 9/2, 7/2\rangle$ state of $4P_{3/2}$. The unusual Rydberg–EIT spectrum in the ladder scheme while scanning the coupling detuning δ_c and locking the probe laser to (a2) SAS and (b2) ultrastable cavity; the normal Rydberg–EIT spectrum scanning the probe detuning δ_p when the coupling laser is fixed, where the probe laser is frequency-locked by the (a3) SAS and (b3) ultrastable cavity. The ladder system is shown as $|g\rangle \rightarrow |e\rangle \rightarrow |r\rangle \equiv |37s\rangle$. The optical density of the remaining atomic sample is normalized to a value of 1 in the absence of the coupling laser. Experimental data in (a2) and (b2) are enlarged by a factor of 3 for comparison with (a3) and (b3) on the same scale. The fitting values for (a1)–(a3) are $\Omega_c = 2\pi \times 11.93$ MHz, $\gamma_{eg} = 2\pi \times 25$ MHz, $\gamma_{rg} = 2\pi \times 12$ MHz, and $\delta_c = 2\pi \times (-1.55)$ MHz. The fitting values for (b1)–(b3) are $\Omega_c = 2\pi \times 11.93$ MHz, $\gamma_{eg} = 2\pi \times 20.1$ MHz, $\gamma_{rg} = 2\pi \times 6.01$ MHz, and $\delta_c = 2\pi \times (-1.48)$ MHz. The red open squares show the experimental data. The solid lines in (a1) and (b1) serve as a guide to the eye. The blue solid curve is the fitting of data to Eq. (1). The red error bars for uncertainties of the EIT lines indicate the standard deviation of three repeated measurements, which come from the stability of the laser's locking and the fluctuations of the atomic number.

$\gamma_{ij} = (\Gamma_i + \Gamma_j)/2 + \gamma_{e(r)}$ includes the natural linewidth of energy level $|i\rangle$ and $|j\rangle$ with $\Gamma_g = 0$ because of the ground state $|g\rangle$, and $\gamma_{e(r)}$ are the decoherence rate, which depends on the laser linewidth and dephasing due to Rydberg interactions[36,57]. Γ_e and Γ_r are the decay rate of the intermediate state $4P_{3/2}$ and Rydberg state, respectively.

Figures 3(a1) and 3(b1) give the spectrum without coupling laser beams by measuring the optical density of remaining atoms in the optical trap as a function of the probe detuning δ_p. There are three dips in the spectrum in Fig. 3(b1), which correspond to the transition from $|F = 9/2\rangle$ state of $4S_{1/2}$ to $|F' = 11/2, 9/2, 7/2\rangle$ states of $4P_{3/2}$, respectively. However, it only displays one dip in Fig. 3(a1), which corresponds to the transition from $|F = 9/2\rangle$ to $|F' = 11/2\rangle$ because of the limited frequency tuning range of the AOM. We find that the full width at half-maximum (FWHM) of the spectral peak in Figs. 3(a1) and 3(b1) is approximately $2\pi \times 20$ MHz.
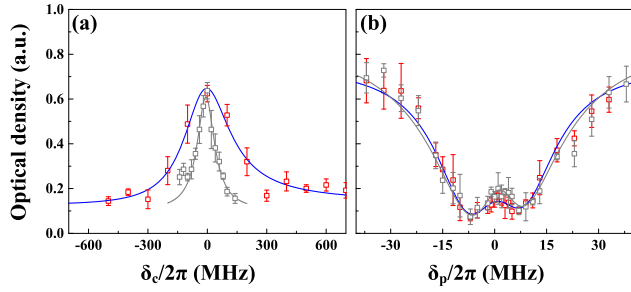
Fig. 4. Observation of the Rydberg–EIT spectrum on 35d Rydberg state. (a) Unusual Rydberg–EIT spectrum (red) while scanning the coupling detuning δ_c and locking the probe laser to ultrastable cavity resonating at the transition from $|g\rangle$ to $|e\rangle$. The Rydberg-EIT spectrum (gray) for 37s Rydberg state is from Figs. 3(b2) and 3(b3). (b) The normal Rydberg–EIT spectrum is obtained by scanning the probe detuning δ_p when the coupling laser is fixed, where the probe laser is frequency-locked through the ultrastable cavity, and the coupling laser is locked to the transition between $|e\rangle$ and $|r\rangle \equiv |35d\rangle$. The fitting values are $\Omega_c = 2\pi \times 14.02$ MHz, $\gamma_{eg} = 2\pi \times 18.5$ MHz, $\gamma_{rg} = 9.5$ MHz, and $\delta_c = 2\pi \times (-0.68)$ MHz.

Fig. 5. Observation of the Rydberg–EIT spectrum on 52s Rydberg state. (a) Unusual Rydberg-EIT spectrum while scanning the coupling detuning δ_c and locking the probe laser to the ultrastable cavity resonating at the transition from $|g\rangle$ to $|e\rangle$. (b) The normal Rydberg–EIT spectrum is obtained by scanning the probe detuning δ_p when the coupling laser is fixed, where the probe laser is frequency-locked through the ultrastable cavity, and the coupling laser is locked to the transition between $|e\rangle$ and $|r\rangle \equiv |52s\rangle$. The fitting values are $\Omega_c = 2\pi \times 6.8$ MHz, $\gamma_{eg} = 2\pi \times 18.5$ MHz, $\gamma_{rg} = 2\pi \times 2.12$ MHz, and $\delta_c = 2\pi \times (-1.92)$ MHz. The red open squares show the experimental data. The red error bars indicate the standard deviation of three repeated measurements. The blue solid curve is the fitting of data to Eq. (1).

Subsequently, the unusual Rydberg–EIT spectrum in the ladder scheme is obtained by scanning the coupling detuning δ_c and locking the probe laser at resonance by saturated absorption spectroscopy (SAS) and ultrastable cavity, as shown in Figs. 3(a2) and 3(b2). The spectrum presents a peak, and the center frequency in the spectrum corresponds to the resonant transition between $|e\rangle$ and $|r\rangle \equiv |37s\rangle$ for the coupling laser. The appearance of the peak in the spectrum is because the strong coupling laser at resonance generates the AC Stark splitting of $|e\rangle$ to reduce the atom loss induced by the resonant probe light.

Then, the normal Rydberg–EIT spectrum is measured by scanning the probe detuning δ_p once the coupling laser is fixed at resonance. Here, the probe laser is frequency-locked by the SAS or the ultrastable cavity as a comparison. The transparency peak appears at the central frequency in the normal Rydberg–EIT spectrum due to the reduced atom loss when the coupling laser is tuned in resonance with a particular Rydberg level, which nicely exhibits the expected transparency resonance in Fig. 3(b3) compared with the Rydberg–EIT spectrum in Fig. 3(a3). The main reason for the difference in the Rydberg–EIT spectrum of Figs. 3(a3) and 3(b3) is the different linewidths of the probe laser with the different locking methods. Here, we show that the linewidth of the probe laser locked to the superstable cavity is narrower than that locked to the SAS by means of the Rydberg–EIT spectrum.

Furthermore, we measure the Rydberg–EIT spectrum with Rydberg state 35d, as shown in Fig. 4. We find that the FWHM ($2\pi \times 250$ MHz) of the spectrum in the unusual Rydberg–EIT spectrum for Rydberg state 35d (red) is larger than the FWHM ($2\pi \times 80$ MHz) of the Rydberg state 37s (gray) in Fig. 4(a). The main reason for the different linewidths is the different DC polarizabilities of the ns and nd states. Here, the polarizability of the nd states is approximately 5 times larger than that of
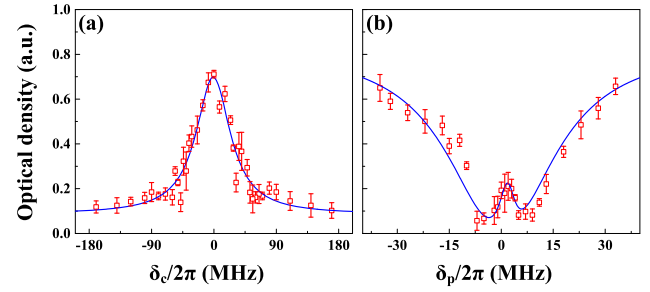
the ns states[58,59], which means that the dipole moment for the transition between the intermediate and the Rydberg state is larger for a D-line than for an S-line.

In addition, we measure the Rydberg–EIT spectrum with the higher Rydberg state 52s, shown in Fig. 5. The height of the transparency peak in a normal Rydberg–EIT spectrum in Fig. 5(b) is higher than the experimental data with 37s, shown in Fig. 3(b3). The enhanced transparency peak observed at smaller γ_{rg} is accurately predicted by Eq. (1). The maximum transparency is thus determined by the linewidth γ_e of the $|g\rangle \rightarrow |r\rangle$ transition and not by the (much broader) linewidth of the $|g\rangle \rightarrow |e\rangle$ transition[60]. Meanwhile, we obtain the linewidth $\gamma_{rg} = 2\pi \times 2.12$ MHz of the $|g\rangle \rightarrow |e\rangle$ transition for the 50s state, which is smaller than that for the 37s state from the fit of Eq. (1). The main reason for this phenomenon is that the coupling strength decreases with the increase of the principal quantum number under a fixed coupling laser intensity. Moreover, it shows that the interaction of the Rydberg-dressed Fermi gas may affect the nature of the transparency peak from these normal Rydberg–EIT spectra, shown in Figs. 3(b3), 4(b), and 5(b), such as reducing the height of the transparency peak and making the transparency peak position shift[61].

4. Conclusion

In conclusion, we measured the Rydberg–EIT spectrum through a two-photon process of the ultracold Fermi ^{40}K atoms in the ladder-type system via scanning probe laser detuning δ_p and coupling laser detuning δ_c, which can be continuously tuned around 3 GHz. We studied the different Rydberg–EIT line shapes when the probe laser is locked to the superstable cavity

and SAS, respectively. We study the Rydberg–EIT line shapes for 37s and 35d states. We also experimentally demonstrate the significant change in the Rydberg–EIT spectrum with different principal quantum numbers of the Rydberg state ($n = 37/52$ and $l = 0$). In addition, we find that the height and width of the transparency peak of the Rydberg–EIT spectrum are determined by the coupling strength, decay rate, and linewidth of the driving-field laser, which is in good agreement with the theoretical prediction. This work provides a platform to obtain higher-resolution hyperfine coupling constant at a higher principal quantum number to probe the properties of interacting Rydberg-dressed atoms and to explore many interesting behaviors involving Rydberg states in ultracold Fermi gases.

Acknowledgement

References

1. T. F. Gallagher, *Rydberg Atoms* (Cambridge University, 1994).
2. M. Saffman, T. G. Walker, and K. Molmer, "Quantum information with Rydberg atoms," Rev. Mod. Phys. **82**, 2313 (2010).
3. W. Li, T. Pohl, J. M. Rost, S. T. Rittenhouse, H. R. Sadeghpour, J. Nipper, B. Butscher, J. B. Balewski, V. Bendkowsky, R. Low, and T. Pfau, "A homonuclear molecule with a permanent electric dipole moment," Science **334**, 1110 (2011).
4. D. Booth, S. T. Rittenhouse, J. Yang, H. R. Sadeghpour, and J. P. Shaffer, "Production of trilobite Rydberg molecule dimers with kilo-Debye permanent electric dipole moments," Science **348**, 99 (2015).
5. S. Hollerith, J. Zeiher, J. Rui, A. Rubio-Abadal, V. Walther, T. Pohl, D. M. Stamper-Kurn, I. Bloch, and C. Gross, "Quantum gas microscopy of Rydberg macrodimers," Science **364**, 664 (2019).
6. H. Saßmannshausen and J. Deiglmayr, "Observation of Rydberg-atom macrodimers: micrometer-sized diatomic molecules," Phys. Rev. Lett. **117**, 083401 (2016).
7. X. Han, S. Bai, Y. Jiao, L. Hao, Y. Xue, J. Zhao, S. Jia, and G. Raithel, "Cs 62D_J Rydberg-atom macrodimers formed by long-range multipole interaction," Phys. Rev. A **97**, 031403(R) (2018).
8. T. Peyronel, O. Firstenberg, Q.-Y. Liang, S. Hofferberth, A. V. Gorshkov, T. Pohl, M. D. Lukin, and V. Vuletić, "Quantum nonlinear optics with single photons enabled by strongly interacting atoms," Nature **488**, 57 (2012).
9. Q.-Y. Liang, A. V. Venkatramani, S. H. Cantu, T. L. Nicholson, M. J. Gullans, A. V. Gorshkov, J. D. Thompson, C. Chin, M. D. Lukin, and V. Vuletic, "Observation of three-photon bound states in a quantum nonlinear medium," Science **359**, 783 (2018).
10. I. Buluta and F. Nori, "Quantum simulators," Science **326**, 108 (2009).
11. H. Weimer, M. Muller, I. Lesanovsky, P. Zoller, and H. P. Buchler, "A Rydberg quantum simulator," Nat. Phys. **6**, 382 (2010).
12. P. Schauß, M. Cheneau, M. Endres, T. Fukuhara, S. Hild, A. Omran, T. Pohl, C. Gross, S. Kuhr, and I. Bloch, "Observation of spatially ordered structures in a two-dimensional Rydberg gas," Nature **491**, 87 (2012).
13. P. Schauß, J. Zeiher, T. Fukuhara, S. Hild, M. Cheneau, T. Macri, T. Pohl, I. Bloch, and C. Gross, "Crystallization in Ising quantum magnets," Science **347**, 1455 (2015).
14. H. Bernien, S. Schwartz, A. Keesling, H. Levine, A. Omran, H. Pichler, S. Choi, A. S. Zibrov, M. Endres, M. Greiner, V. Vuletic, and M. D. Lukin, "Probing many body dynamics on a 51-atom quantum simulator," Nature **551**, 579 (2017).
15. M. Morgado and S. Whitlock, "Quantum simulation and computing with Rydberg-interacting qubits," AVS Quantum Sci. **3**, 023501 (2021).
16. X. Wu, X. Liang, Y. Tian, F. Yang, C. Chen, Y.-C. Liu, M. K. Tey, and L. You, "A concise review of Rydberg atom based quantum computation and quantum simulation," Chin. Phys. B **30**, 020305 (2021).
17. M. Saffman, "Quantum computing with atomic qubits and Rydberg interactions: progress and challenges," J. Phys. B **49**, 202001 (2016).
18. L. Henriet, L. Beguin, A. Signoles, T. Lahaye, A. Browaeys, G.-O. Reymond, and C. Jurczak, "Quantum computing with neutral atoms," Quantum **4**, 327 (2020).
19. T. C. Liebisch, M. Schlagmuller, F. Engel, H. Nguyen, J. Balewski, G. Lochead, F. Bottcher, K. M. Westphal, K. S. Kleinbach, T. Schmid, A. Gaj, R. Low, S. Hoffer berth, T. Pfau, J. Pérez-Ríos, and C. H. Greene, "Controlling Rydberg atom excitations in dense background gases," J. Phys. B **49**, 182001 (2016).
20. J. Sous, H. R. Sadeghpour, T. C. Killian, E. Demler, and R. Schmidt, "Rydberg impurity in a Fermi gas: quantum statistics and rotational blockade," Phys. Rev. Res. **2**, 023021 (2020).
21. R. Heidemann, U. Raitzsch, V. Bendkowsky, B. Butscher, R. Low, and T. Pfau, "Rydberg excitation of Bose-Einstein condensates," Phys. Rev. Lett. **100**, 033601 (2008).
22. M. Viteau, M. Bason, J. Radogostowicz, N. Malossi, O. Morsch, D. Ciampini, and E. Arimondo, "Rydberg excitation of Bose-Einstein condensates," Laser Phys. **23**, 015502 (2013).
23. M. Viteau, M. Bason, J. Radogostowicz, N. Malossi, O. Morsch, D. Ciampini, and E. Arimondo, "Rydberg excitation of Bose-Einstein condensates," Laser Phys. **23**, 015502 (2013).
24. S. Hollerith, J. Zeiher, J. Rui, A. Rubio-Abadal, V. Walther, T. Pohl, D. M. Stamper-Kurn, I. Bloch, and C. Gross, "Quantum gas microscopy of Rydberg macrodimers," Science **364**, 664 (2019).
25. J. Zeiher, J.-Y. Choi, A. Rubio-Abadal, T. Pohl, R. van Bijnen, I. Bloch, and C. Gross, "Coherent many-body spin dynamics in a long-range interacting ising chain," Phys. Rev. X **7**, 041063 (2017).
26. V. Borish, O. Marković, J. A. Hines, S. V. Rajagopal, and M. Schleier-Smith, "Transverse-field Ising dynamics in a Rydberg-dressed atomic gas," Phys. Rev. Lett. **124**, 063601 (2020).
27. J. Zeiher, R. van Bijnen, P. Schauß, S. Hild, J.-Y. Choi, T. Pohl, I. Bloch, and C. Gross, "Many-body interferometry of a Rydberg-dressed spin lattice," Nat. Phys. **12**, 1095 (2016).
28. B. Xiong, H. H. Jen, and D.-W. Wang, "Topological superfluid by blockade effects in a Rydberg-dressed Fermi gas," Phys. Rev. A **90**, 013631 (2014).
29. A. Keleş, E. Zhao, and X. Li, "f-wave superfluidity from repulsive interaction in Rydberg-dressed Fermi gas," Phys. Rev. A **101**, 023624 (2020).
30. R. Khasseh, S. H. Abedinpour, and B. Tanatar, "Phase diagram and dynamics of Rydberg-dressed fermions in two dimensions," Phys. Rev. A **96**, 053611 (2017).
31. M. Mattioli, M. Dalmonte, W. Lechner, and G. Pupillo, "Cluster Luttinger liquids of Rydberg-dressed atoms in optical lattices," Phys. Rev. Lett. **111**, 165302 (2013).
32. W.-H. Li, T.-C. Hsieh, C.-Y. Mou, and D.-W. Wang, "Emergence of a metallic quantum solid phase in a Rydberg-dressed Fermi gas," Phys. Rev. Lett. **117**, 035301 (2016).
33. X. Li and S. D. Sarma, "Exotic topological density waves in cold atomic Rydberg-dressed fermions," Nat. Commun. **6**, 7137 (2015).
34. D. Li, G. Bian, J. Miao, P. Wang, Z. Meng, L. Chen, L. Huang, and J. Zhang, "Rydberg excitation spectrum of ^{40}K ultracold Fermi gases," Phys. Rev. A **103**, 063305 (2021).
35. E. Guardado-Sanchez, B. M. Spar, P. Schauss, R. Belyansky, J. T. Young, P. Bienias, A. V. Gorshkov, T. Iadecola, and W. S. Bakr, "Quench dynamics of a Fermi gas with strong nonlocal interactions," Phys. Rev. X **11**, 021036 (2021).

36. K. J. Weatherill, J. D. Pritchard, R. P. Abel, M. G. Bason, A. K. Mohapatra, and C. S. Adams, "Electromagnetically induced transparency of an interacting cold Rydberg ensemble," J. Phys. B **41**, 201002 (2008).

37. M. Fleischhauer, A. Imamoglu, and J. P. Marangos, "Electromagnetically induced transparency: optics in coherent media," Rev. Mod. Phys. **77**, 633 (2005).

38. K.-J. Boller, A. Imamoglu, and S. E. Harris, "Observation of electromagnetically induced transparency," Phys. Rev. Lett. **66**, 2593 (1991).

39. C. Y. Ye and A. S. Zibrov, "Width of the electromagnetically induced transparency resonance in atomic vapor," Phys. Rev. A **65**, 023806 (2002).

40. A. F. Monden, "EIT spectroscopy on rubidium Rydberg states," Master's thesis (Eindhoven University of Technology, 2015).

41. B. Yang, Q. Liang, J. He, T. Zhang, and J. Wang, "Narrow-linewidth double-resonance optical pumping spectrum due to electromagnetically induced transparency in ladder-type inhomogeneously broadened media," Phys. Rev. A **81**, 043803 (2010).

42. B. Yang, J. Gao, T. Zhang, and J. Wang, "Electromagnetically induced transparency without a Doppler background in a multilevel ladder-type cesium atomic system," Phys. Rev. A **83**, 013818 (2011).

43. A. Krishna, K. Pandey, A. Wasan, and V. Natarajan, "High-resolution hyperfine spectroscopy of excited states using electromagnetically induced transparency," Europhys. Lett. **72**, 221 (2005).

44. R. Cardman and G. Raithel, "Hyperfine structure of $nP_{1/2}$ Rydberg states in ^{85}Rb," Phys. Rev. Lett. **106**, 052810 (2013).

45. S. C. Bell, D. M. Heywood, J. D. White, J. D. Close, and R. E. Scholten, "Laser frequency offset locking using electromagnetically induced transparency," Appl. Phys. Lett. **90**, 171120 (2007).

46. R. P. Abel, A. K. Mohapatra, M. G. Bason, J. D. Pritchard, K. J. Weatherill, U. Raitzsch, and C. S. Adams, "Laser frequency stabilization to excited state transitions using electromagnetically induced transparency in a cascade system," Appl. Phys. Lett. **94**, 071107 (2009).

47. A. K. Mohapatra, T. R. Jackson, and C. S. Adams, "Coherent optical detection of highly excited Rydberg states using electromagnetically induced transparency," Phys. Rev. Lett. **98**, 113003 (2007).

48. S. Mauger, J. Millen, and M. P. A. Jones, "Spectroscopy of strontium Rydberg states using electromagnetically induced transparency," J. Phys. B **40**, F319 (2007).

49. J. Zhao, X. Zhu, L. Zhang, Z. Feng, C. Li, and S. Jia, "High sensitivity spectroscopy of cesium Rydberg atoms using electromagnetically induced transparency," Opt. Express **17**, 15821 (2009).

50. S. Chai, P. Wang, Z. Fu, L. Huang, and J. Zhang, "The design of a dipole traps for Bose-Einstein condensate and degenerate Fermi gas," Acta Sin. Quantum Opt. **18**, 171 (2012).

51. L. Chen, G. Yang, Z. Meng, L. Huang, and P. Wang, "Electromagnetically induced transparency in ^{87}Rb Bose Einstein condensate," J. Quantum Opt. **23**, 246 (2017).

52. N. Sibalić, J. Pritchard, C. Adams, and K. Weatherill, "Spectroscopy of strontium Rydberg states using electromagnetically induced transparency," J. Phys. B **40**, F319 (2007).

53. J. I. Thorpe, K. Numata, and J. Livas, "Laser frequency stabilization and control through offset sideband locking to optical cavities," Opt. Express **16**, 15980 (2008).

54. J. Han, T. Vogt, M. Manjappa, R. Guo, M. Kiffner, and W. Li, "Lensing effect of electromagnetically induced transparency involving a Rydberg state," Phys. Rev. A **92**, 063824 (2015).

55. A. Tebben, C. Hainaut, A. Salzinger, S. Geier, T. Franz, T. Pohl, M. Garttner, G. Zürn, and M. Weidemüller, "Nonlinear absorption in interacting Rydberg electromagnetically-induced-transparency spectra on two-photon resonance," Phys. Rev. A **103**, 063710 (2021).

56. J. D. Pritchard, "Cooperative optical non-linearity in a blockaded Rydberg ensemble," Ph.D. thesis (Durham University, 2011).

57. H. M. M. Alotaibi and B. C. Sanders, "Double-double electromagnetically induced transparency with amplification," Phys. Rev. A **89**, 021802 (2014).

58. A. Arias, S. Helmrich, C. Schweiger, L. Ardizzone, G. Lochead, and S. Whitlock, "Versatile, high-power 460 nm laser system for Rydberg excitation of ultracold potassium," Opt. Express **25**, 14829 (2017).

59. G. Yang, L. Chen, C. Mi, P. Wang, and J. Zhang, "Electromagnetically induced transparency and electromagnetically induced absorption in ^{87}Rb Bose-Einstein condensate," J. Quantum Opt. **24**, 156 (2018).

60. J. E. Field, K. H. Hahn, and S. E. Harris, "Observation of electromagnetically induced transparency in collisionally broadened lead vapor," Phys. Rev. Lett. **67**, 3062 (1991).

61. J. Han, T. Vogt, and W. Li, "Spectral shift and dephasing of electromagnetically induced transparency in an interacting Rydberg gas," Phys. Rev. A **94**, 043806 (2016).